



Imaging the Geometry of Cimandiri Fault Zone Based on 2D Audio-Magnetotelluric (AMT) Model in Nyalindung, Sukabumi–Indonesia

ILHAM ARISBAYA,^{1,2} LINA HANDAYANI,¹ MARUF M. MUKTI,¹ YAYAT SUDRAJAT,¹ HENDRA GRANDIS,² and PRIHADI SUMINTADIREJA³

Abstract—We present an interpretation of newly acquired audio-magnetotelluric data to reveal the subsurface geometry of Cimandiri Fault Zone, one of the major active faults in the western part of Java. The line section is 25 km long in a nearly north–south direction across the axes of CFZ with 24 stations of 750–1200 m spacing intervals. The 2D AMT inversion model shows two conductive zones in the southern part that may be associated to the Miocene rocks of the Southern Mountains, and a conductive zone in the northern part that is likely to be associated with Gunung Walat fold-belt. The subsurface structures of the Southern Mountains are dominated by south-dipping thrusts that may uplift the shallow marine sediments. Shallow seismicity occurred around CFZ indicating the activity of these blind thrusts.

Key words: Cimandiri Fault Zone, audio-magnetotelluric, Indonesia.

1. Introduction

Surface characterization of a fault zone geometry in humid areas where faults were buried by thick sediments or soils is challenging (Marliyani et al. 2016). Erosion-sedimentation process, high anthropogenic activity, and intensive agricultural activity would likely make the surface fault manifestations hard to be recognized (e.g., Louis et al. 2002). Moreover, surface rupture is difficult to observe if the structures are dominated by blind faults where shortening in the near surface is accommodated by

folding rather than fault slip (Dolan et al. 2003; Hubbard and Shaw 2009). The devastating 2011 M 7.1 Van earthquake (Turkey) was sourced from a blind fault in the Van Fault Zone (Elliott et al. 2013) and shows us that blind thrusts are such an important source of major earthquakes.

Active geophysical surveys such as seismic reflection, electrical resistivity tomography, and ground penetrating radar have been proven to be suitable methods for imaging subsurface structures (Hubbard et al. 2010; Natawidjaja et al. 2017; Pueyo Anchueta et al. 2016; Syukri and Saad 2017). However, data acquisition of active-source geophysical methods in a densely populated area is more complicated (mostly in logistic and human impact). Therefore, the application of passive geophysical methods in imaging subsurface structures geometry is needed in such areas. Gravity and magnetic surveys can be used as a preliminary study to map the lateral boundary of changes in physical properties of rocks (Pueyo Anchueta et al. 2016). However, modeling these two methods to produce a vertical cross-section requires a priori model and a depth control as a constraint to reduce model ambiguity (e.g., Davy et al. 2013). Electromagnetic methods had been commonly used to determine the configuration of subsurface resistivity in a fault zone without a priori model (Mekkawi and Saleh 2007; Tank 2014; Yamaguchi et al. 2010).

Cimandiri Fault Zone (CFZ), one of the major active faults in western Java, stretches along 100 km through a densely populated area (Dardji et al. 1994; Marliyani et al. 2016). This fault zone had been recognized as east–west trending linear features in satellite imagery and topographic map along

¹ Research Center for Geotechnology, Indonesian Institute of Sciences (LIPI), Bandung 40135, Indonesia. E-mail: ilham.arisbaya@lipi.go.id

² Geophysical Engineering, Institut Teknologi Bandung (ITB), Bandung 40132, Indonesia.

³ Geological Engineering, Institut Teknologi Bandung (ITB), Bandung 40132, Indonesia.

Cimandiri valley. The southern block appears to have been uplifted relative to the northern block (Sudjatmiko 1972; Sukanto 1975) (Fig. 1). The Southern Mountain block has been interpreted to have initially formed farther south of its present position and developed toward north due to the propagation of thrust faults (Clements et al. 2009). The frontal limit of the thrust faults is speculated to be parallel with the northern boundary of the Jampang Formation along Cimandiri Valley. This deformation has been interpreted to have occurred during the early or middle

Miocene and the fault has been considered to be no longer active today.

An offshore extension of this fault zone had been reported farther southwest based on observation of seismic reflection data (Malod et al. 1995; Susilohadi et al. 2005). A paleostress study concluded that the western part of this fault zone formed a left-lateral strike-slip fault (Dardji et al. 1994). Regional magnetotelluric (MT) model shows different basement rocks characters between the north and the south side of the Cimandiri River, thus the western part of the CFZ has been interpreted as a strike-slip fault zone

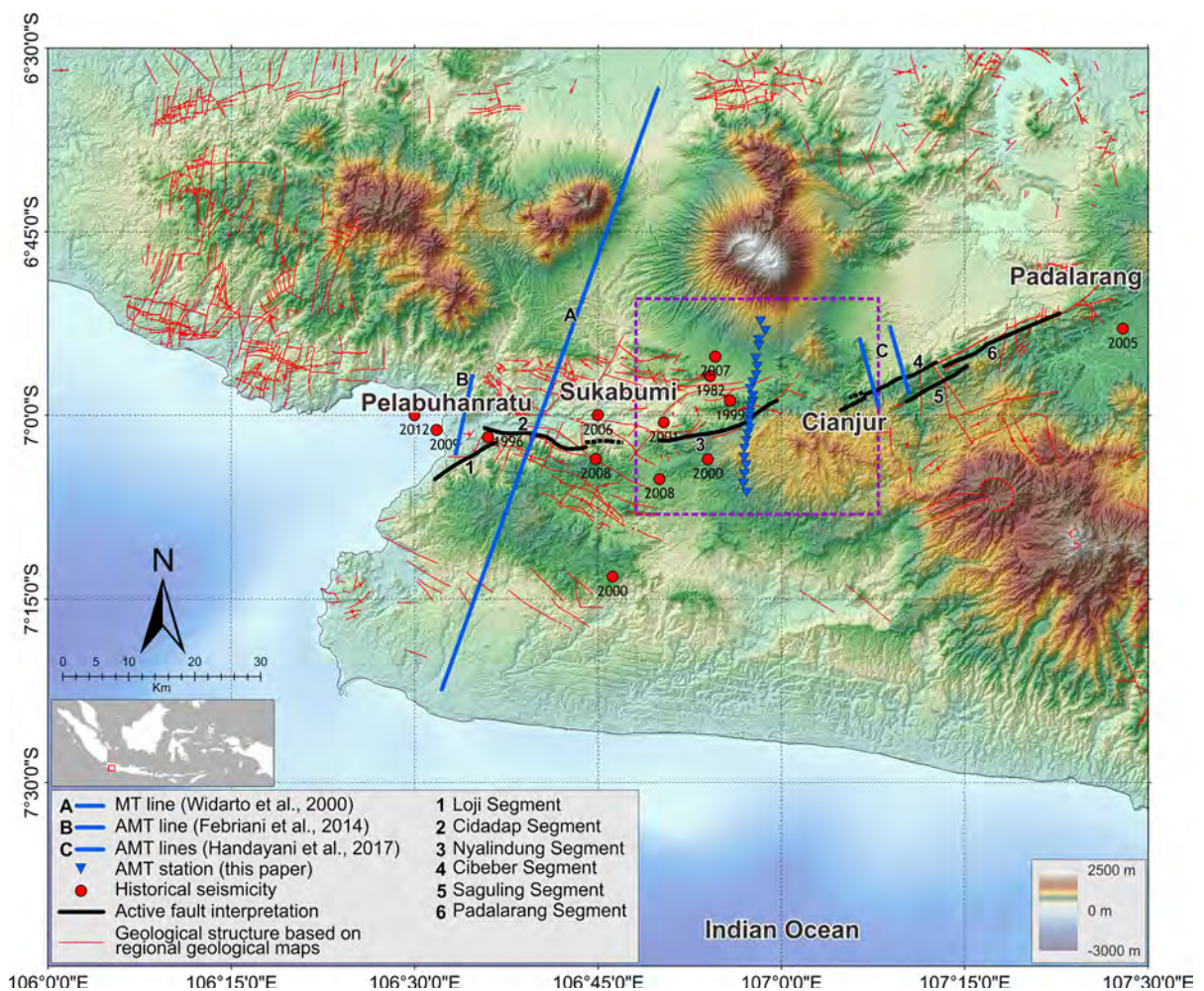


Figure 1

CFZ as an active fault is marked by thick black line and divided into six segments (Marliyani et al. 2016). Geological structures are from Effendi et al. (1998), Koesmono et al. (1996), Sudjatmiko (1972), Sukanto (1975). Historical seismicity around the CFZ are from Marliyani et al. (2016); Supartoyo et al. (2006); Visser (1922). Dashed Purple Square indicate the blow up map in Fig. 2

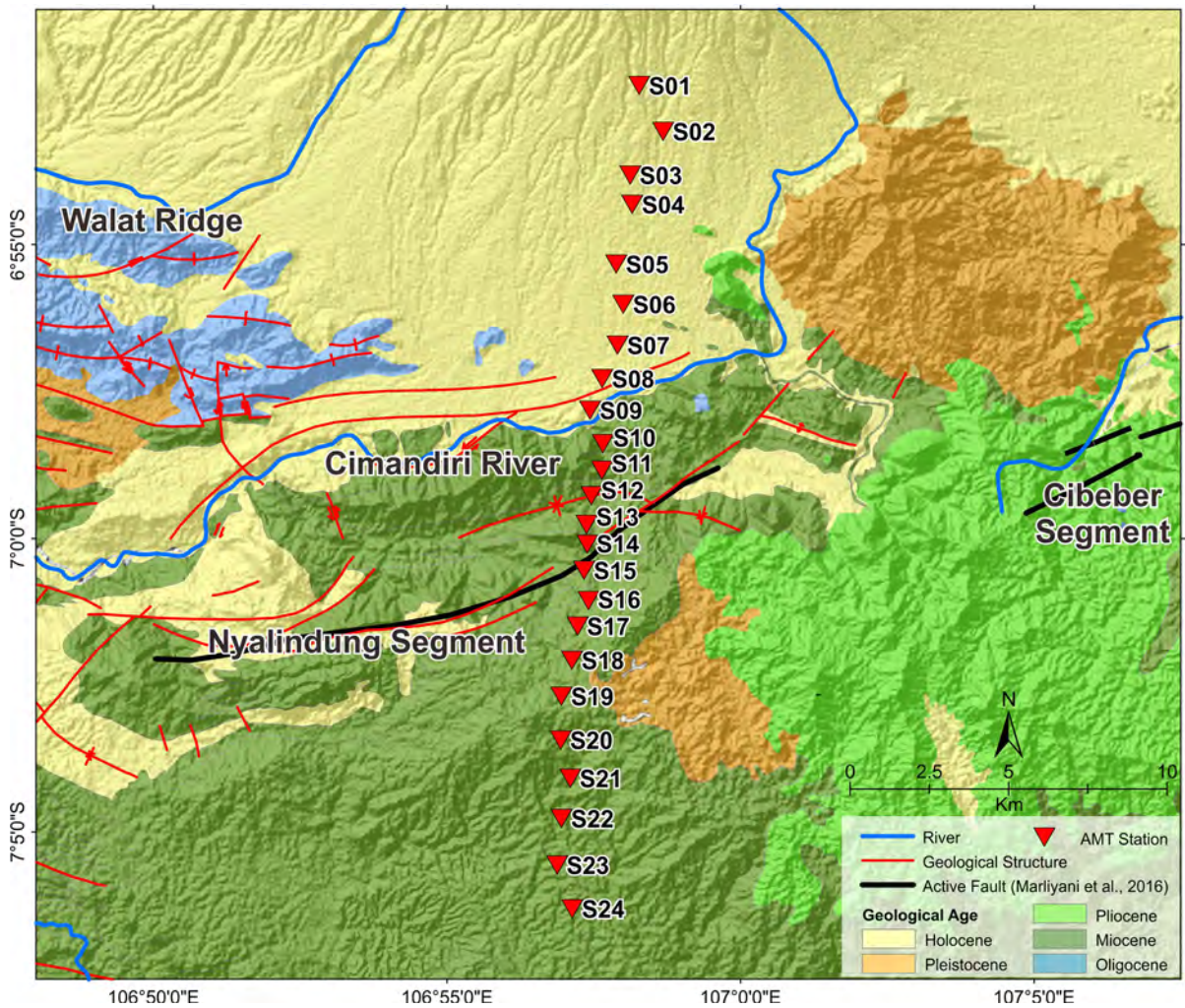


Figure 2

Regional geological map of research area based on rocks age (simplified from Effendi et al. 1998; Koesmono et al. 1996; Sudjatmiko 1972; Sukanto 1975). The red reversed triangles (S01–S24) are the location of AMT stations, crossing Cimandiri River and Nyalindung Segment

(Widarto et al. 2000). Recent audio-magnetotelluric (AMT) model around Pelabuhanratu Bay shows a discontinuity zone with a slope dipping to the south (Febriani et al. 2013). Therefore the geometry of the CFZ is more favorable to be classified as a thrust fault.

The eastern part of this fault zone that extends from Cianjur to Padalarang forms a SW-NE trend thrust-fault belt (Sudjatmiko 1972). Recently acquired AMT data crossing the eastern part of CFZ imaged several folds involving Middle Miocene sediments, and a thrust fault covered by the river

alluvial deposits in Cibeber Segment (Handayani et al. 2017). Therefore, the two-dimensional (2D) AMT model around Pelabuhanratu Bay (Febriani et al. 2013) shows similar result to that of the AMT model in Cibeber (Handayani et al. 2017), each associated with the western and eastern part of CFZ respectively.

A number of studies conducted in CFZ, especially in the western and eastern part of this fault zone, have shed new perspectives on neotectonic processes in this area. However, the central part of CFZ marks the changes of the fault trending direction, from W–E in

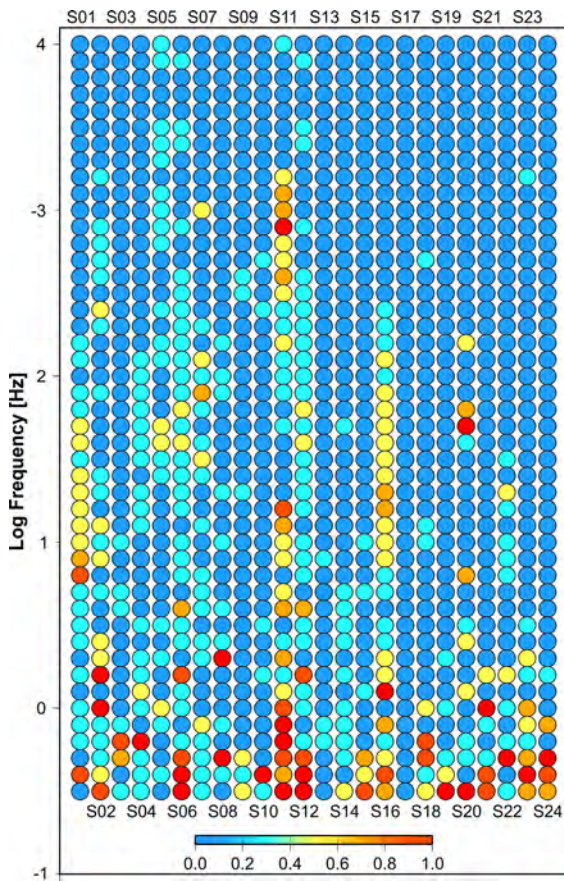


Figure 3

Plot of skew angle (β) of all AMT Nyalindung measuring points in all frequency ranges. The vertical axis shows the frequency (in log scale) and the color scale shows the skew angle (β), which indicates the dimensionality of the regional conductivity structure

the west to NE–SW in the east. The geometry and mechanism of the fault in this central part remain unclear. Therefore, we investigated the subsurface geometry of the central part of CFZ to understand the origin of its formative process. In this paper, we report our 2D AMT data modeling in Nyalindung, Sukabumi to image the subsurface geometry of the central part of CFZ.

2. Geological Setting

Java is often cited as an example of the product of orthogonal subduction along the Sunda active margin, and structural configuration along this island is assumed to be a relatively simple structure. The

physiographic zone proposed by van Bemmelen (1949), which also represents structural units, is elongated along the axis of the island parallel to the trench. In the northern part, the trace of a major thrust-fold belt of Baribis-Kendeng Fault (BKF) has been observed along the island that extends farther east to the Flores Thrust (Clements et al. 2009; Silver et al. 1986; Simandjuntak and Barber 1996). To the south, another major fault zone, the Lembang Fault (LF) is observed as a left-lateral strike-slip fault (Afnimar et al. 2015; Daryono et al. 2018), nearly parallel to the BKF (Dam et al. 1996; Katili 1970; Meilano et al. 2012). In the western part of Java, the other major fault systems are recognized as SW-trending Cimandiri Fault Zone (CFZ) and the NW-trending Citandui Fault Zone (CtFZ), and both have wrench component of movement (Dardji et al. 1994; Simandjuntak and Barber 1996). The trace of CFZ was observed trending E–W direction in the western part and ENE–WSW in the eastern part. The offshore extension of this fault zone was observed in a seismic reflection section farther southwest in Pelabuanratu Bay (Malod et al. 1995; Susilohadi et al. 2005).

Geological field observations in the fault zone have suggested that CFZ was developed as a strike-slip fault. Based on the stratigraphic observation of Paleogene rocks in the western Java, a regional petroleum geologic study has proposed that CFZ was likely to develop as a thrust fault that is no longer active (Clements et al. 2009). A recent active-fault study showed that CFZ is an active left-lateral reverse (oblique) fault divided by six segments: Loji, Cidap, Nyalindung, Saguling, and Padalarang (Marliyani et al. 2016) (see Fig. 1).

A 3-year campaign of GPS survey in CFZ has revealed that the fault zone experienced horizontal movement with varying directions and rates ranging from 0.5 to 1.7 cm/year (Abidin et al. 2009). Based on an observation of fault scarps in CFZ, the fault zone was then classified as a low slip-rate fault (Marliyani et al. 2016) that might be associated with an extended period of earthquake ruptures. Further active-fault research in the CFZ is hindered by the thick volcanic and marine Neogene sediment covers (van Bemmelen 1949; Effendi et al. 1998; Koesmono et al. 1996; Sudjatmiko 1972; Sukamto 1975).

3. Methods

The audio-magnetotelluric (AMT) survey is appropriate for delineating fault zones, because the presence of fluid in the fracture zone may cause a decrease in the resistivity value of the host rock (Becken et al. 2011; Mekkawi and Saleh 2007; Yamaguchi et al. 2010). We carried out AMT measurement with a frequency range of 1 Hz–10 kHz to image the shallow (~ 2 km) subsurface resistivity configuration.

The survey was conducted using the Phoenix MTU5a instrument. The natural electric field was measured using two pairs of porous-pots as dipoles with a length of 60 m in N–S/W–E direction (E_x and E_y). Each porous-pot was buried in a 30 cm deep hole to stabilize the contact with the ground which was maintained below 1000 Ωm . The natural magnetic field was measured by induction coils (H_x and H_y) which were buried in the ground to maintain a stable position during measurement. Both electric field and magnetic field sensors were placed about 30 m from the main unit. The electromagnetic (EM) field was measured simultaneously and coordinated in universal time systems based on GPS. During our field campaign in 2016, we did AMT measurement at a total of 24 stations (S01–S24), with 750–1200 m interval between stations, in approximately 25 km of nearly north–south line (Fig. 2). AMT measurement for each station took a minimum of 1.5 h. The first station, S01 was located in the north on the foothill of Gede-Pangrango volcano, and the last station, S24, was in a hilly area in the south. The Central part of the line is a valley where the Cimandiri River is located.

Field data processing was conducted using SSMT200 and MT-editor software package. This initial data processing included calibration process, time series data transformation into the frequency domain, robust processing, and cross-power selection. In the latter, the coherence level of the EM signal is increased by masking on the noisy data, leading to a smoother apparent resistivity and phase curve.

In MT method, the conductivity structure, i.e. dimensionality, can be studied based on some parameters of the data, such as skew angle, ellipticity,

and polar diagram analysis (Simpson and Bahr 2005). Here we used the classical Swift skew angle (β) method to analyze the dimensionality of the data and geoelectric strike (Z-strike) direction. The method uses a value of 0.2 as a cut-off, greater skew values might be an indication of three-dimensional (3D) heterogeneity effect or near surface distortion.

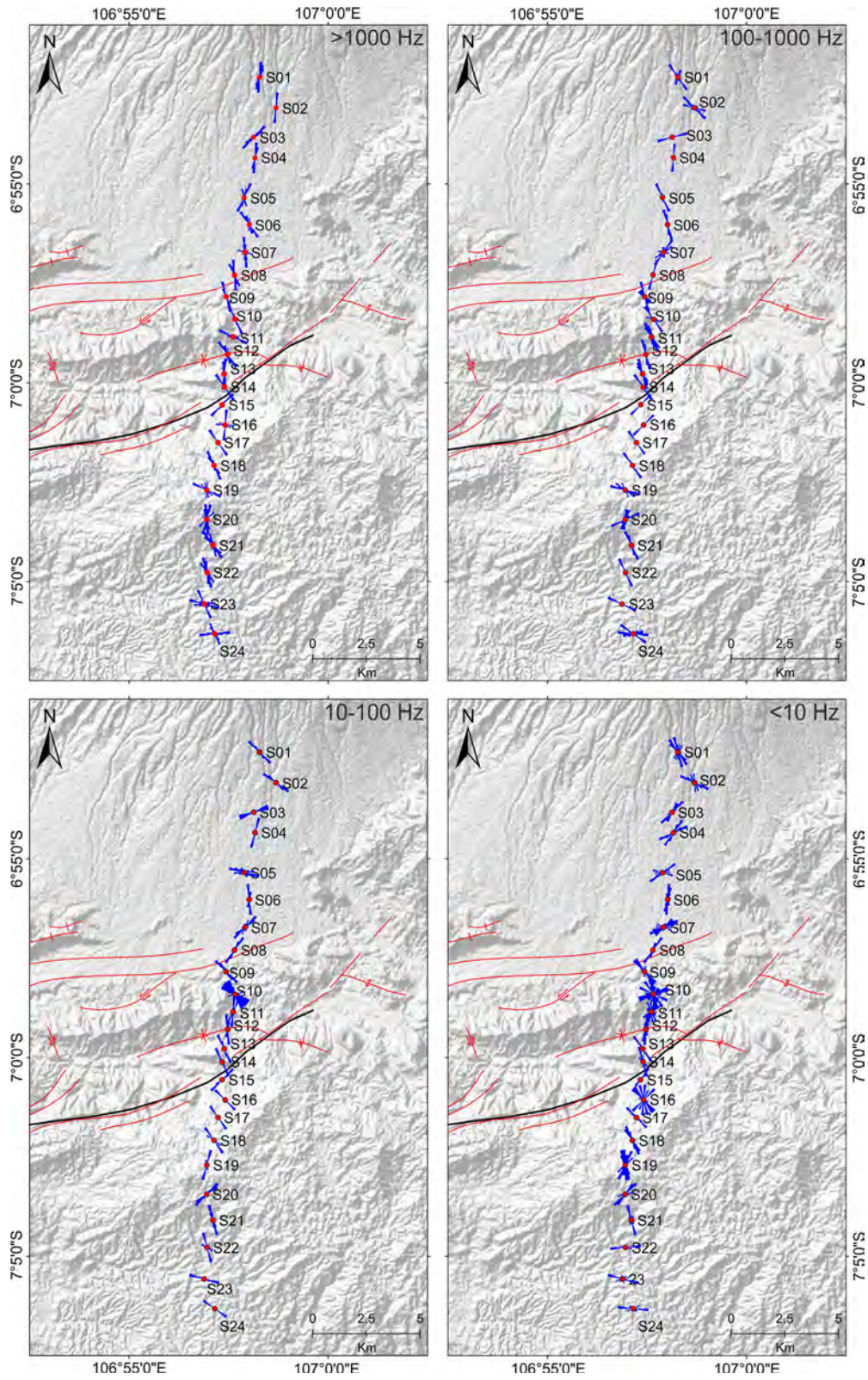
The impedance tensor in two-dimensional (2D) MT modelling should be rotated to the regional geoelectric strike axis in order to minimize the diagonal component (Z_{xx} and Z_{yy}) prior to inversion process. CFZ as the object of this research has a relatively obvious direction, which is almost W–E (Febriani et al. 2013; Handayani et al. 2017; Marliyani et al. 2016), thus the distribution of measuring stations has been adjusted to be almost in a N–S line. The impedance tensor analysis, i.e. rotation, aims to confirm the geoelectric strike changes along the line. Therefore, the rose diagram plot is depicted for each station. After rotation, the apparent resistivity component that was obtained with electric field parallel to the geoelectric strike is referred to as TE mode. The other one which was obtained with magnetic field parallel to the geoelectric strike is referred to as TM mode.

The TE and TM mode apparent resistivity and phase were then used to perform 2D inverse modeling. The inversion was done by using WinGLink software package, which used the nonlinear conjugate gradient (NLCG) algorithm (Rodi and Mackie 2001). The inversion started with an initial model of uniform half-space of 100 Ωm with the horizontal grid cell size approximately 250 m and error floor of 5%. In the NLCG algorithm, the regularization parameter is used as a trade-off between the data misfit and the model smoothness. In this modeling, the value of three was used for the regularization parameter.

4. Results

4.1. Skew Angles

Most of the obtained data (70%) exhibit skew angles below 0.2° , and 27.9% of the data are in the interval of 0.2° – 1° (Fig. 3). High skew values ($> 1^\circ$)



◀Figure 4

Rose diagram of Z-strike from all AMT sites at four frequency ranges (> 1000 Hz, $100\text{--}1000$ Hz, $10\text{--}100$ Hz, and < 10 Hz). The red lines shows the fault interpretation in the regional geological map, while the black line is active fault interpretation (Marliyani et al. 2016)

are observed mainly in low frequencies with a percentage of 2.2% of the total data obtained and indicates 3D conductivity in the deeper part of the subsurface. High skew angles are also observed at higher frequencies of some stations located close to the residential housing. We speculate that the MT data quality on these stations were affected by intensive anthropogenic noises, which then affects the actual skew angle value. With most of the data showing a low skew-angle value, and only a small fraction with high skew-angle value, we concluded that the AMT data obtained in Nyalindung could be modeled in 2D, especially at high frequencies.

4.2. Z-Strike

The geoelectric strike analysis determined the direction of resistivity structure that can be used to infer geological features that may not be visible on the surface. The Z-strike angle of the Nyalindung AMT data varies between measuring stations and frequencies (Fig. 4). At high frequencies (> 100 Hz), the rose diagram of Z-strike at most measuring stations indicates a general trend toward north–south (N–S) direction. At low frequencies (< 100 Hz), the Z-strike rose diagram is more varied, but the main trend can still be observed as north northwest–south southeast (NNW–SSE) direction. The varied Z-strike direction at low frequencies implies that the geoelectric structure is 3-D at the deeper part as indicated by the skew angle. Some measuring stations show different Z-strike direction which appears in west–east (W–E) direction. However, the N–S and W–E directions may depict the same geoelectric strike feature considering the nature of 90° ambiguity of Z-strike.

Cimandiri Fault is observed to be curved (or bend) in Nyalindung segment. However, this N35E angle surface expression seems to be a more local feature rather than a regional one. Overall, the

Z-strikes of all data are consistent across all frequencies. We chose WSW–ENE as the structural direction which is orthogonal to NNW–SSE indicated by Zstrike considering the 90° ambiguity. Furthermore, we adopted the general direction of Cimandiri Fault, which is almost W–E, and take N80E as the geoelectric strike angle as did Febriani et al. (2013).

4.3. Apparent Resistivity

The curve of the apparent resistivity and its phase of some AMT measuring stations are in Fig. 5. Most of the stations in the northern part of the study area (S01–S13) show a typical apparent resistivity curve of which the value keeps increasing, except for S03 and S04, which decrease to a minimum and return to increase in the lower frequency. The northern part of the research area is dominated by high apparent resistivity, particularly at S05. The apparent resistivity at this station shows a value of more than $50,000 \Omega\text{m}$. Since it is located close to residential housing, this extremely high apparent resistivity value was thought to be affected by intensive anthropogenic noises. However, the high apparent resistivity value pattern was confirmed by the adjacent measuring stations, S06 and S07, which range up to $4,000 \Omega\text{m}$. Low apparent resistivity values were observed in S03 and S04, that is $< 150 \Omega\text{m}$ and $< 250 \Omega\text{m}$ respectively, in contrast to the surrounding measurement stations which reached $1000 \Omega\text{m}$. Noting the curve type and apparent resistivity value that differs from the surrounding stations, these two stations indicate a localized anomaly and may reflect narrow subsurface feature.

The southern part (S14–S24) is dominated by low-value apparent resistivity which increases at a frequency of 1 Hz. At S16 and S17, the apparent resistivity curve increases at around 100 Hz, while at S20 and S21, it increases at 10 Hz. Some stations data show a large error bar in the lower frequency, they are S01, S02, S06, S07, S10, S11, S21, S22, and S24. Since a large error bar would affect the inversion process and result, the data span was limited to 1 Hz for these data.

A qualitative interpretation of subsurface structures has been performed by analyzing the apparent resistivity and phase pseudo-Section (Fig. 6). The

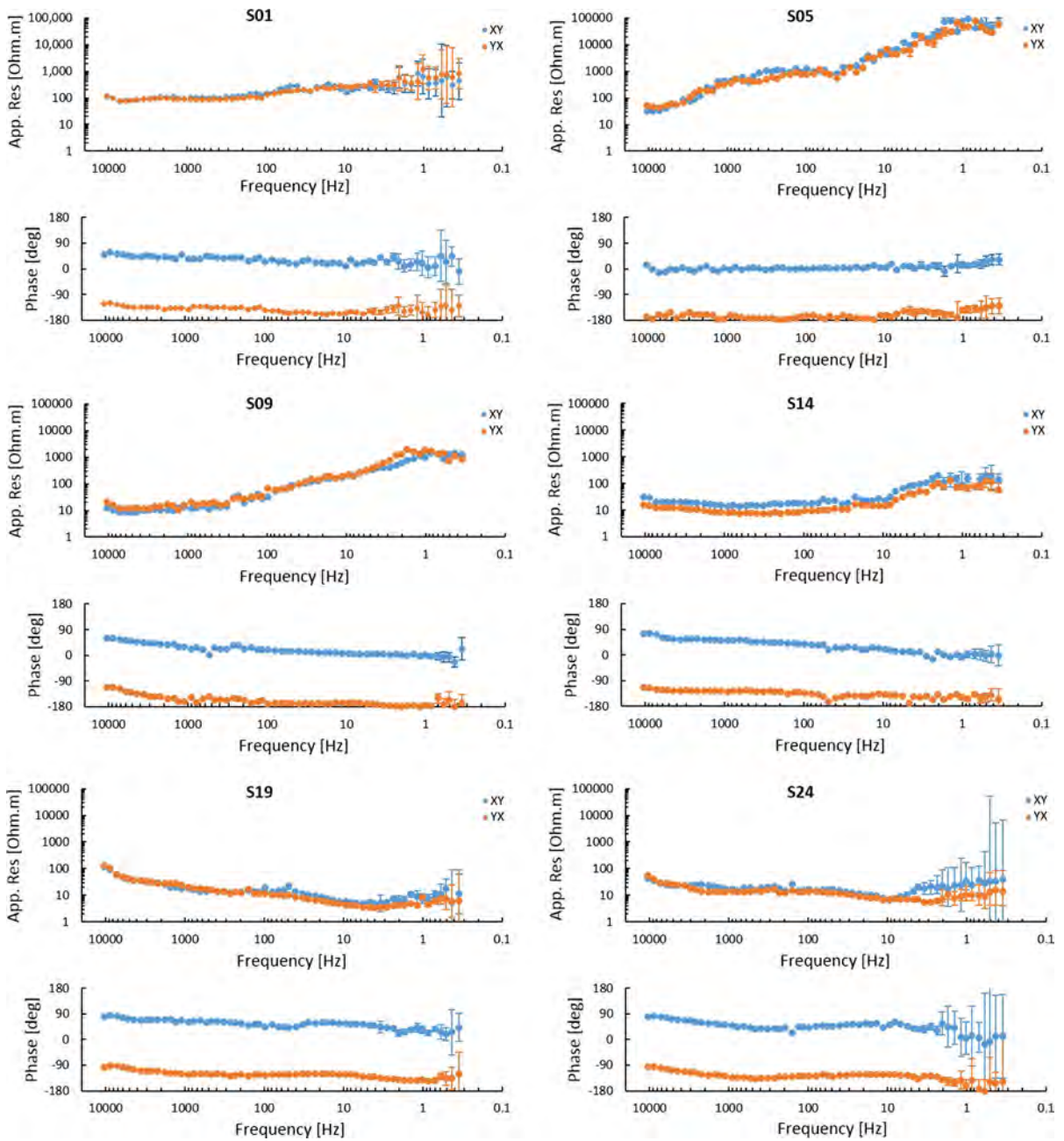


Figure 5
Apparent resistivity and impedance phase curves at S01, S05, S09, S14, S19, and S24 measuring stations

most striking feature in the pseudo-section is the presence of the low apparent resistivity values ($< 64 \Omega\text{m}$) at high frequency in the central part of the line, S06–S16. This low apparent resistivity feature is observed continuously to the south as the

frequency decreases, while high apparent resistivity values ($> 1000 \Omega\text{m}$) are observed in the northern part of the line at low frequency. The intermediate apparent resistivity value ($64\text{--}1000 \Omega\text{m}$) is dominant in the north and only observed at the high-frequency

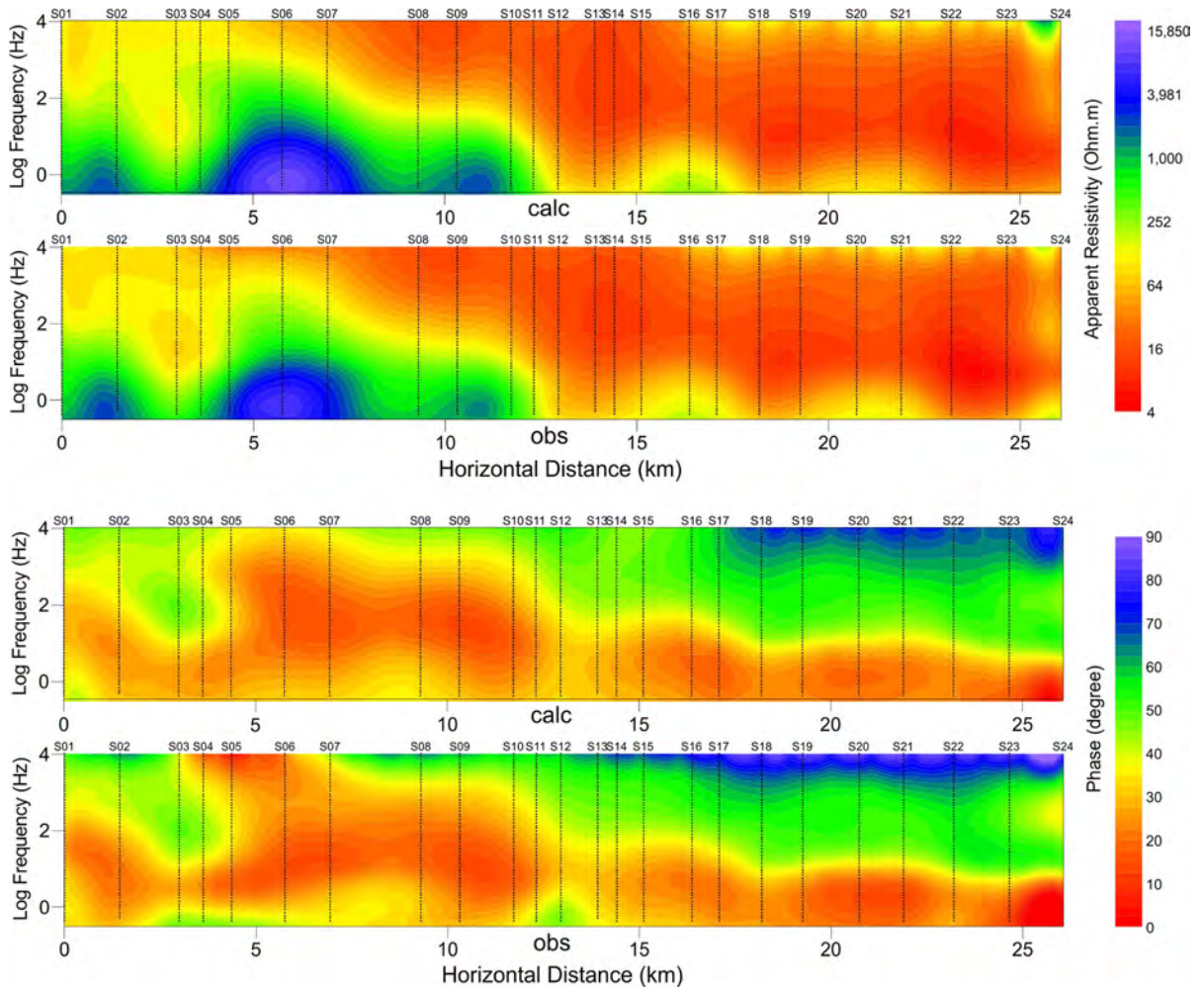


Figure 6

Pseudo-sections of apparent resistivity and impedance phase from measurement (obs.) and model (calc.) for all measuring stations. Black dots indicate data position at each measuring station

range in the south. The southward dipping pattern is also observed in the impedance phase pseudo-section. However, the phase pseudo-section is more difficult to be correlated with the structure.

4.4. Inversion Modeling

The result from 2D inversion modeling shows similar feature to the pseudo-Section (Fig. 6). The 2D inversion model was divided into three groups based on the resistivity value. The first group has a low resistivity with the value below $60 \Omega\text{m}$ (purple–light blue), the second group has value between 60 and

$1000 \Omega\text{m}$ (light green–dark green), and the third group has value more than $1000 \Omega\text{m}$ (yellow–red) (Fig. 7). This 2D resistivity model appears to be in good agreement with the geological information, where Cimandiri valley is largely covered by volcanic rocks and fluvial, to shallow marine sediments (Sukanto 1975). In the near-surface layer, there is a significant difference between the northern and southern part of the profile. The southern part is dominated by a very low resistivity ($< 60 \Omega\text{m}$) rocks observed to a depth of about 1 km, here referred to as K1 and K2. Low resistivity values are commonly associated with high porosity and high fluid content.

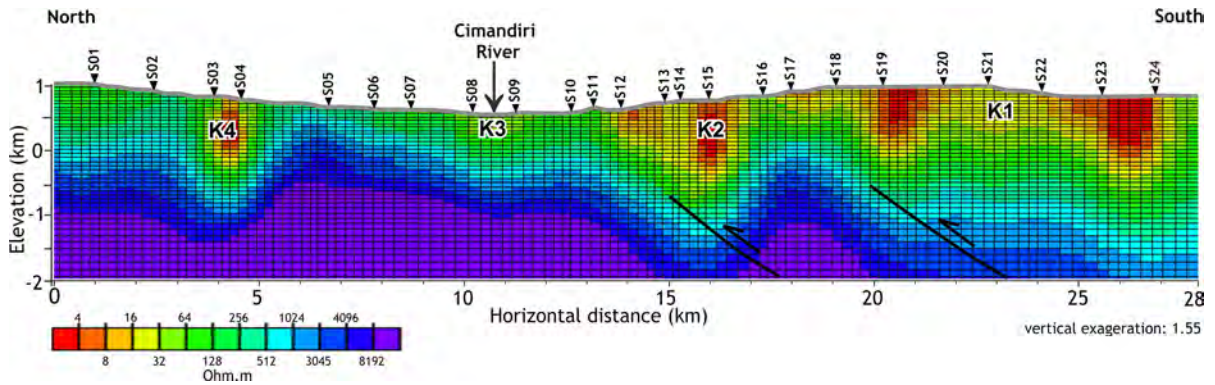


Figure 7

Subsurface resistivity structures interpretation of Nyalindung segment based on AMT data. K1, K2, K3, and K4 are conductive (low resistivity) zones

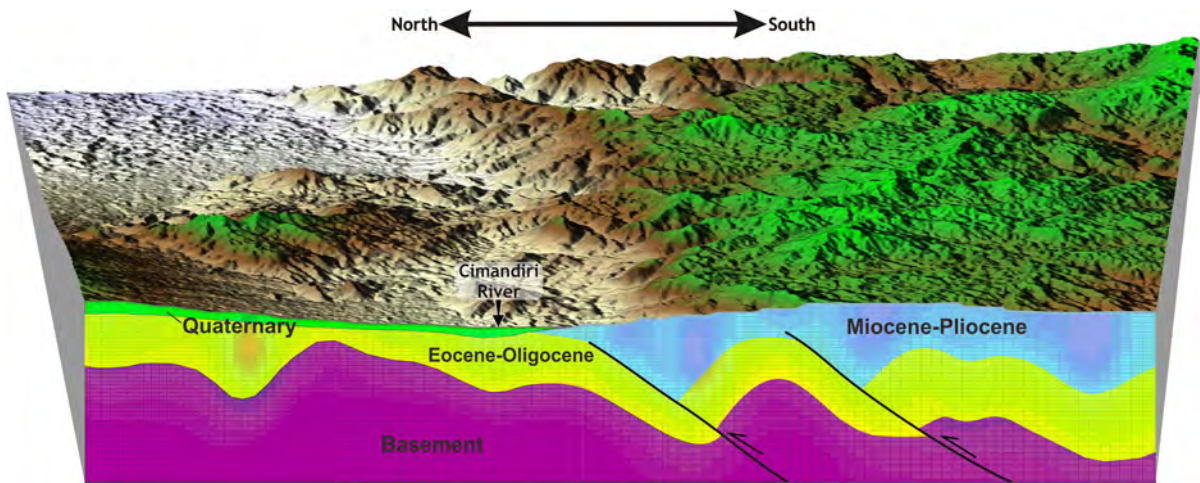


Figure 8

Sketch of the subsurface structural configuration in the central part of CFZ based on the 2D resistivity model results, shows two thrust faults that uplifted the Miocene-Pliocene shallow marine sediments toward north. The perspective map is from SRTM30 image

Therefore, we interpreted these low resistivity values as unconsolidated sediments or highly-fractured rocks.

In the northern part of the profile, the near-surface resistivity model shows a low to moderate resistivity value (60–1000 Ωm). These values may be associated with young volcanic rocks overlying the Eocene–Oligocene fluvial sediments. This medium resistivity layer seems to be deepened to the south of the profile. A thin layer with low resistivity value is also observed in the central part of the line around Cimandiri River (K3), and it can be associated with alluvial deposit in the valley morphology. A very low

conductive zone is also observed in the northern part of the profile between S03 and S04 (K4). The resistive zone ($> 1000 \Omega\text{m}$) is interpreted as a basement at a depth of more than 1000 m from the surface. The basement shows a relatively undulated horizon and deepened to the south.

5. Discussion

The conductive zones of K1 and K2 in the southern part of the section are occupied by the Miocene shallow marine sediments and volcanics of

Jampang Formation that were exposed with undulated morphology (Koesmono et al. 1996). The exposures of these Miocene rocks suggests a Middle-Late Miocene uplift (Schiller et al. 1991) or a thrust-fault belt development (Clements et al. 2009). The intense deformation endured by these rocks might have enhanced the porosity that generally leads to lower resistivity values. The conductive zone of K4 in the northern area appears to be more vertically oriented with the basement in the southern block being uplifted higher than that of the northern part. This observation can be attributed to the folds of Walat Ridges that trend in east–west direction (Effendi et al. 1998) located to the west of the K4 conductive zone.

If K1 and K2 were interpreted as Jampang Formation, then there would be two scenarios of geological structures that separated the two conductive bodies. The first scenario is that K1 and K2 were separated by a southern basement undulation that appears as a restraining bend that produced “positive flower structure”. Jampang Formation that was uplifted at the top of the restraining bend was then eroded. This structural feature usually appears in the step-over area between two strike-slip fault segments. However, our AMT line was located in the Nyalindung Segment, not in the step-over section.

The second scenario is that there are two thrust faults located beneath the southern part of the line. The first thrust fault is located in the southern part that appears to cut and separate conductive bodies K1 and K2. If this reverse fault continued up to the surface, this fault could be observed between S15 and S16. At the same location, Marliyani et al. (2016) has proposed the Nyalindung Segment that stretches along 19 km in ENE–WSW direction. The second thrust fault is located in the central part around Cimandiri valley (K3). This resistivity contrast is covered by a low resistivity layer, which is interpreted as alluvium deposition around Cimandiri River.

Former AMT surveys near Pelabuhanratu Bay and across Cibeber Segment (B and C in Fig. 1) revealed thrust geometry of CFZ (Febriani et al. 2013; Handayani et al. 2017), while regional MT survey in Cidadap Segment (A Fig. 1) showed slightly different subsurface models (Widarto et al.

2000). However, if we focus on the features of the MT model only up to 2 km depth, the model also shows marine sediments around the CFZ at the near surface and dipping to the south. Such observation could also be interpreted as a reverse fault dipping to the south. The basement in the northern block shows higher resistivity that can be interpreted as fluvio-deltaic rocks environment, whereas the relatively lower resistivity layer in the southern block is associated with deeper marine sedimentary rocks as hypothesized by Clements et al. (2009). Taking into account the position of the AMT line, and the results of previous AMT surveys on the nearby segments, we argue that the second scenario (there are two thrust faults located beneath the southern part of the line) is more likely than the first scenario. Sketch of geological model based on 2D resistivity model is shown in Fig. 8.

The 2D AMT model of Nyalindung Segment shows that the basement in the southern part of the line has a deeper position than the northern part. This indicates that in the original conditions, the southern part was in a deeper environment. The model also showed that the medium resistivity layer is thickening southward. It can be interpreted that this layer is formed in a basin environment, which was then uplifted by the thrust fault. Both thrust faults mapped in our model accommodated northward deformation regionally occurred in the area.

Previous work argued that CFZ is not an active fault because its surface rupture could not be observed in the SRTM (Shuttle Radar Topography Mission) image (Clements et al. 2009). Our resistivity model shows the existence of the thrust faults, one of them is between S10 and S11, which coincide with CFZ at the surface. The fault’s continuity to the surface could not be ascertained due to the thick sediment covers. However, the occurrence of recent shallow earthquakes around CFZ (Abidin et al. 2009; Marliyani et al. 2016; Supartoyo et al. 2006; Visser 1922) indicates the possibility that these thrusts are active blind faults. Further research is required at near-surface depth to obtain a more detailed geometry description of this active fault.

6. Conclusions

We have shown the resistivity subsurface model of Nyalindung Segment of CFZ based on AMT data. This segment is a central part of the fault zone and shows the changes in the fault trending direction, from W–E in the west to NE–SW in the east. The resistivity model revealed the existence of two thrust features dipping to the south. These reverse faults might be related to the deformation that uplifted the shallow marine sediments to the current elevation. Both thrusting features are located at a depth of more than 500 m and do not reach the surface. However, the historical seismicity in this area can be an indication that the thrusts are active blind faults.

Acknowledgements

This research is part of a thematic research with funding sources from annual research budget of Research Center for Geotechnology LIPI. Greatest gratitude is expressed to the landowners who allowed us to take AMT measurements on their land. We thank our Geophysics Field Team: Sunardi, Nyanjang, Sutarman, and Dede Rusmana. We also express our gratitude to the editor and two anonymous reviewers for their input and constructive comments that greatly improved this paper.

Publisher's Note Springer Nature remains neutral with regard to jurisdictional claims in published maps and institutional affiliations.

REFERENCES

- Abidin, H. Z., Andreas, H., Kato, T., Ito, T., Meilano, I., Kimata, F., Natawidjaya, D. H., & Harjono, H. (2009). Crustal deformation studies in Java (Indonesia) using GPS. *Journal of Earthquake and Tsunami*, *03*, 77–88. <https://doi.org/10.1142/S1793431109000445>.
- Afnimar, Yulianto, E., & Rasmid (2015). Geological and tectonic implications obtained from first seismic activity investigation around Lembang fault. *Geoscience Letters* *2*, 11. <https://doi.org/10.1186/s40562-015-0020-5>.
- Becken, M., Ritter, O., Bedrosian, P. A., & Weckmann, U. (2011). Correlation between deep fluids, tremor and creep along the San Andreas fault. *Nature*, *480*, 87–90. <https://doi.org/10.1038/nature10609>.
- Clements, B., Hall, R., Smyth, H. R., & Cottam, M. A. (2009). Thrusting of a volcanic arc: a new structural model for Java. *Petroleum Geoscience*, *15*, 159–174. <https://doi.org/10.1144/1354-079309-831>.
- Dam, M. A. C., Suparan, P., Nossin, J. J., & Voskuil, R. (1996). A chronology for geomorphological developments in the greater Bandung area, West-Java, Indonesia. *Journal of Southeast Asian Earth Sciences*, *14*, 101–115. [https://doi.org/10.1016/S0743-9547\(96\)00069-4](https://doi.org/10.1016/S0743-9547(96)00069-4).
- Dardji, N., Villemint, T., & Rampnoux, J. P. P. (1994). Paleostresses and strike-slip movement: the cimandiri fault zone, West Java, Indonesia. *Journal of Southeast Asian Earth Sciences*, *9*, 3–11. [https://doi.org/10.1016/0743-9547\(94\)90061-2](https://doi.org/10.1016/0743-9547(94)90061-2).
- Daryono, M. R., Natawidjaja, D. H., Sapiie, B., & Cummins, P. (2018). Earthquake geology of the lembang fault, West Java, Indonesia. *Tectonophysics*, *751*, 180–191. <https://doi.org/10.1016/j.tecto.2018.12.014>.
- Davy, R., Stern, T., & Townend, J. (2013). Gravity analysis of glaciotectonic processes, central alpine fault, South Island, New Zealand. *New Zealand Journal of Geology and Geophysics*, *56*, 100–108. <https://doi.org/10.1080/00288306.2013.782324>.
- Dolan, J. F., Christofferson, S. A., & Shaw, J. H. (2003). Recognition of paleoearthquakes on the puente hills blind thrust fault, California. *Science*, *300*, 115–118. <https://doi.org/10.1126/science.1080593>.
- Effendi, A. C., Kusnama, & Hermanto, B. (1998). *Geological map of the Bogor quadrangle, Java*. Bandung: Geological Research and Development Centre.
- Elliott, J. R., Copley, A. C., Holley, R., Scharer, K., & Parsons, B. (2013). The 2011 Mw7.1 Van (Eastern Turkey) earthquake. *Journal of Geophysical Research: Solid Earth*, *118*, 1619–1637. <https://doi.org/10.1002/jgrb.50117>.
- Febriani, F., Hattori, K., Widarto, D. S., Han, P., Yoshino, C., Nurdianto, B., Effendi, N., Maulana, I., & Gaffar, E. (2013). Audio Frequency Magnetotelluric Imaging of the Cimandiri Fault, West Java, Indonesia. *Jurnal Geofisika*. *14*(1), 131–143.
- Handayani, L., Maryati, M., Kamtono, K., Mukti, M. M., & Sudrajat, Y. (2017). Audio-magnetotelluric modeling of cimandiri fault zone at Cibeber, Cianjur. *Indonesian Journal on Geoscience*, *4*, 39–47. <https://doi.org/10.17014/ijog.4.1.39-47>.
- Hubbard, J., & Shaw, J. H. (2009). Uplift of the Longmen Shan and Tibetan plateau, and the 2008 Wenchuan (M = 7.9) earthquake. *Nature*, *458*, 194–197. <https://doi.org/10.1038/nature07837>.
- Hubbard, J., Shaw, J. H., & Klinger, Y. (2010). Structural setting of the 2008 Mw7.9 Wenchuan, China, earthquake. *Bulletin of the Seismological Society of America*, *100*, 2713–2735. <https://doi.org/10.1785/0120090341>.
- Katili, J. A. (1970). Large transcurrent faults in Southeast Asia with special reference to Indonesia. *Geologische Rundschau*, *59*, 581–600. <https://doi.org/10.1007/BF01823809>.
- Koesmono, M., Kusnama, & Suwarna, N. (1996). *Geological map of the Sindangbarang and Bandarwaru quadrangle, Java*. Bandung: Geological Research and Development Centre.
- Louis, I. F., Raftopoulos, D., Goullis, I., & Louis, F. I. (2002). Geophysical imaging of faults and fault zones in the Urban. In *International Conference on Earth Sciences and Electronics* (pp. 269–285).
- Malod, J. A., Karta, K., Beslier, M. O., & Zen, M. T. (1995). From normal to oblique subduction: tectonic relationships between Java and Sumatra. *Journal of Southeast Asian Earth Sciences*, *12*, 85–93. [https://doi.org/10.1016/0743-9547\(95\)00023-2](https://doi.org/10.1016/0743-9547(95)00023-2).

- Marliyani, G. I., Arrowsmith, J. R., & Whipple, K. X. (2016). Characterization of slow slip rate faults in humid areas: cimandiri Fault zone, Indonesia. *Journal of Geophysical Research*, *121*, 2287–2308. <https://doi.org/10.1002/2016JF003846>.
- Meilano, I., Abidin, H. Z., Andreas, H., Gumilar, I., Sarsito, D., Hanifa, N. R., Rino, Harjono, H., Kato, T., Kimata, F., & Fukuda, Y. (2012). Slip rate estimation of the Lembang Fault West Java from geodetic observation. *Journal of Disaster Research*, *7*, 12–18. <https://doi.org/10.20965/jdr.2012.p0012>.
- Mekkwawi, M., & Saleh, A. (2007). Case studies of magnetotelluric method applied to mapping active faults. *Acta Geodaetica et Geophysica Hungarica*, *42*, 383–397. <https://doi.org/10.1556/AGeod.42.2007.4.2>.
- Natawidjaja, D. H., Bradley, K., Daryono, M. R., Aribowo, S., & Herrin, J. (2017). Late Quaternary eruption of the Ranau Caldera and new geological slip rates of the sumatran fault zone in Southern Sumatra, Indonesia. *Geoscience Letters*, *4*, 15. <https://doi.org/10.1186/s40562-017-0087-2>.
- Pueyo Anchuela, Ó., Lafuente, P., Arlegui, L., Liesa, C. L., & Simón, J. L. (2016). Geophysical characterization of buried active faults: the concud fault (Iberian Chain, NE Spain). *International Journal of Earth Sciences*, *105*, 2221–2239. <https://doi.org/10.1007/s00531-015-1283-y>.
- Rodi, W. L., & Mackie, R. L. (2001). Nonlinear conjugate gradients algorithm for 2-D magnetotelluric inversion. *Geophysics*, *66*, 1–38. <https://doi.org/10.1190/1.1444893>.
- Schiller, D. M., Garrard, R. A., & Prasetyo, L. (1991). Eocene submarine fan sedimentation in southwest Java. In *Proceedings 20th annual convention of Indonesian Petroleum Association* (pp. 125–182).
- Silver, E. A., Breen, N. A., Prasetyo, H., & Hussong, D. M. (1986). Multibeam study of the flores backarc thrust belt, Indonesia. *Journal of Geophysical Research*, *91*, 3489–3500. <https://doi.org/10.1029/JB091iB03p03489>.
- Simandjuntak, T. O., & Barber, A. J. (1996). Contrasting tectonic styles in the Neogene orogenic belts of Indonesia. In R. Hall & D. Blundell (Eds.), *Tectonic evolution of Southeast Asia, geological society special publication No. 106* (pp. 185–201). London: Geological Society of London. <https://doi.org/10.1144/gsl.sp.1996.106.01.12>.
- Simpson, F., & Bahr, K. (2005). *Practical Magnetotellurics*. Cambridge: Cambridge University Press. <https://doi.org/10.1017/CBO9780511614095>.
- Sudjarmiko, S. (1972). *Geological map of the Cianjur quadrangle, Java*. Bandung: Geological Research and Development Centre.
- Sukanto, R. A. B. (1975). *Geological map of the Jampang-Balekambang quadrangle, Java*. Bandung: Geological Research and Development Centre.
- Supartoyo, Putranto, E. T., Djadja (2006). *Earthquake hazard zone map of Indonesia, 3rd edn*. Bandung: Center for Volcanology and Geological Hazard Mitigation.
- Susilohadi, S., Gaedicke, C., & Ehrhardt, A. (2005). Neogene structures and sedimentation history along the Sunda forearc basins off southwest Sumatra and southwest Java. *Marine Geology*, *219*, 133–154. <https://doi.org/10.1016/j.margeo.2005.05.001>.
- Syukri, M., & Saad, R. (2017). Seulimeum segment characteristic indicated by 2-D resistivity imaging method. *NRIAG Journal of Astronomy and Geophysics*, *6*, 210–217. <https://doi.org/10.1016/j.nrjag.2017.04.001>.
- Tank, S. B. (2014). Fault zone conductors in Northwest Turkey inferred from audio frequency magnetotellurics. *Earth Planets Space*, *64*, 729–742. <https://doi.org/10.5047/eps.2012.02.001>.
- van Bemmelen, R. W. (1949). *The geology of Indonesia*. The Hague: Govt. Printing Office.
- Visser, S. W. (1922). *Inland and submarine epicenter of Sumatra and Java earthquakes*. Batavia: Javasche Boekhandel en Drukkerij.
- Widarto, D. S., Trisukmono, D., Sudrajat, Y., & Sumantri, I. (2000). Citra Tahanan Jenis Magnetotelurik Lintasan Jampang Kulon-Bogor Memotong Zona Sesar Cimandiri, Jawa Barat. In *Proceedings of Research Center for Geotechnology, Indonesian Institute of Sciences (LIPI)*, (pp. 7–28).
- Yamaguchi, S., Ogawa, Y., Fuji-ta, K., Ujihara, N., Inokuchi, H., & Oshiman, N. (2010). Audio-frequency magnetotelluric imaging of the hijima fault, Yamasaki fault system, southwest Japan. *Earth Planets Space*, *62*, 401–411. <https://doi.org/10.5047/eps.2009.12.007>.

(Received January 14, 2019, revised May 29, 2019, accepted June 3, 2019)